IOP Publishing Journal of Physics: Condensed Matter
J. Phys.: Condens. Matter **36** (2024) 393002 (12pp) https://doi.org/10.1088/1361-648X/ad5ad0

Topical Review

Open-circuit voltage deficits in Tin-based perovskite solar cells

Xue Ma and Ning Wang*

College of Physics, Jilin University, Changchun 130012, People's Republic of China

E-mail: ningwang@jlu.edu.cn

Received 19 April 2024, revised 10 June 2024
Accepted for publication 21 June 2024
Published 2 July 2024

Abstract

The power conversion efficiency of Pb-based single-junction perovskite solar cells (PSCs) has surpassed 26%; however, the biocompatibility concerns associated with Pb pose threats to both the environment and living organisms. Consequently, the development of Pb-free PSCs is imperative. Among the various alternatives to Pb-based PSCs, Sn-based PSCs have exhibited outstanding optoelectronic properties, showing great potential for large-scale manufacturing and commercialization. Nevertheless, there remains a significant efficiency gap between Sn-based and Pb-based PSCs. The disparity primarily stems from substantial open-circuit voltage (V_{OC}) deficits in Sn-based PSCs, typically ranging from 0.4 to 0.6 V. The main reason of V_{OC} deficits is severe non-radiative recombination losses, which are caused by the uncontrolled crystallization kinetics of Sn halide perovskites and the spontaneous oxidation of Sn^{2+}. This review summarizes the reasons for V_{OC} deficits in Sn-based PSCs, and the corresponding strategies to mitigate these issues. Additionally, it outlines the persistent challenges and future prospects for Sn-based PSCs, providing guidance to assist researchers in developing more efficient and stable Sn-based perovskites.

Keywords: Sn-based PSCs, V_{OC} deficit, nonradiative recombination, crystallization kinetics, V_{Sn} defects

1. Introduction

Perovskites are characterized by high light absorption coefficients [1], high carrier mobility [2], long carrier diffusion lengths [3], low exciton binding energy [4], and tunable bandgaps [5]. These outstanding optoelectronic properties make perovskites be one of the most promising candidates for the third-generation photovoltaic techniques. The general formula for metal halide perovskite is ABX_3 [6–8], where A mainly consists of alkali metal (Na^+, K^+, or Cs^+), or organic ($CH_3NH_3^+$, MA^+ or $HC(NH_2)_2^+$, FA^+) cations, B consists of divalent metal cations (Pb^{2+}, Sn^{2+}, or Ge^{2+}), and X consists of halide anions (I^-, Br^-, or Cl^-) [9]. The three-dimensional crystal structure is formed by connecting $[BX_6]^{4-}$ octahedra through corner sharing, while the A-site cations occupy the interstitial positions of the octahedral [10]. Since Kojima *et al* first applied $MAPbI_3$ perovskite to dye-sensitized cells and achieved a power conversion efficiency (PCE) of 3.8% in 2009 [11], the certified efficiency of $FA_{1-x}Cs_xPbI_3$ perovskite solar cells (PSCs) has reached 25.7% in 2023 [12].

However, considering the biocompatibility issues associated with Pb that may contaminate soil and pose risks to flora and fauna, reducing or completely eliminating Pb is of paramount importance. Consequently, many researchers have focused on replacing Pb with other less toxic metal elements, identifying Sn as one of the most promising candidates due to its similar ionic radius (Sn^{2+}, 110 pm; Pb^{2+},

* Author to whom any correspondence should be addressed.

Table 1. Summary of high-efficiency Sn-based PSCs.

Composition	Device structure	V_{OC} (V)	J_{SC} (mA cm^{-1})	FF (%)	PCE (%)	References
$EA_{0.1}FA_{0.9}Sn_{0.95}Ge_{0.05}I_3$	ITO/PEDOT: PSS/Perovskite/C_{60}/BCP/Ag	0.84	20.32	78	13.24	[17]
$FASnI_3$	ITO/PEDOT: PSS/Perovskite/C_{60}/C_{60}-BPy/BCP/Ag	0.82	23.45	73.1	14.14	[18]
$FASnI_3$	ITO/PEDOT: PSS/Perovskite/C_{60}/BCP/Ag	0.77	24.9	76.7	14.7	[19]
$(Cs_{0.025}(MA_{0.25}FA_{0.75})_{0.975})_{0.98}EDA_{0.01}SnI_3$	ITO/PEDOT: PSS/Perovskite/C_{60}/BCP/Ag	0.825	23.84	73.74	14.41	[20]
$(MA_{0.25}FA_{0.75})_{0.98}EDA_{0.01}SnI_{2.99}(BF_4)_{0.01}$	ITO/PEDOT: PSS/Perovskite/C_{60}/BCP/Ag	0.81	23.47	74.05	14.08	[21]
$FASnI_3$	ITO/PEDOT: PSS/Perovskite/C_{60}/BCP/Ag	0.817	22.49	77.4	14.23	[22]
$FASnI_3$	ITO/PEDOT: PSS/Perovskite/C_{60}/BCP/Cu	0.8	24.2	73.5	14.2	[23]
$PEA_{0.15}FA_{0.85}SnI_3$	ITO/PEDOT: PSS/Perovskite/ICBA/BCP/Ag	0.94	17.4	75	12.4	[24]
$PEA_{0.15}FA_{0.85}SnI_{2.85}Br_{0.15}$	ITO/PEDOT: PSS/Perovskite/ICBA/BCP/Ag	0.84	20.11	80.26	13.55	[25]
$PEA_{0.15}FA_{0.85}SnI_{2.85}Br_{0.15}$	ITO/PEDOT: PSS/Perovskite/ICBA/BCP/Ag	0.93	19.66	74.9	13.70	[26]
$PEA_{0.15}FA_{0.85}SnI_{2.85}Br_{0.15}$	ITO/PEDOT: PSS/Perovskite/ICBA/BCP/Ag	0.91	20.6	77.1	14.63	[27]
$FASnI_3$	ITO/PEDOT: PSS/Perovskite/ICBA/BCP/Ag	0.92	20.4	76.7	14.3	[28]
$FPEA_{0.15}FA_{0.85}SnI_3$	ITO/PEDOT: PSS/Perovskite/ICBA/BCP/Ag	0.84	24.91	70.76	14.81	[29]
$PEA_{0.2}FA_{0.8}SnI_{2.85}Br_{0.15}$	ITO/PEDOT: PSS/Perovskite/ICBA/BCP/Ag	1.013	18.89	73.21	14.02	[30]
$PEA_{0.15}FA_{0.85}SnI_{2.3}$	ITO/PEDOT: PSS/Perovskite/fullerene/BCP/Ag	0.9	21.39	75.7	14.58	[31]
$PEA_{0.15}FA_{0.85}SnI_{2.3}$	ITO/PEDOT: PSS/Perovskite/fullerene/BCP/Ag	0.856	24.81	72.37	15.35	[32]
$FASnI_3$	ITO/PEDOT: PSS/Perovskite/ICBA/BCP/Ag	0.974	21.4	74.1	15.7	[33]

119 pm) and electronic configuration (ns^2 np^2), which enable the formation of a stable perovskite structure [13]. The optical bandgap of Pb-based perovskites is 1.5–1.7 eV, while that of Sn-based perovskites is 1.2–1.4 eV, closer to the ideal optical bandgap (1.34 eV) for the Shockley–Queisser limit under 1.5 AM solar spectrum [14–16]. This allows Sn-based PSCs to have a higher theoretical open-circuit voltage (V_{OC}) than Pb-based PSCs. However, the V_{OC} of Sn-based PSCs is significantly lower than their optical bandgap, resulting from severe photon energy loss (E_{loss}) (0.4–0.6 eV). According to the equation: $E_{loss} = E_g - qV_{OC}$ (where E_g is the bandgap and q is the elementary charge), E_{loss} is closely related to the V_{OC}. Thus, understanding the V_{OC} loss is crucial for improving the photovoltaic performance of Sn-based PSCs.

Previous review articles have primarily summarized the research progress, challenges, and corresponding strategies for Sn-based PSCs. Table 1 present the device structures and relevant device parameters of Sn-based PSCs reported in recent years. This overview offers a unique perspective by focusing on the mechanisms behind the V_{OC} deficit in Sn-based PSCs, while highlighting the potential of Sn-based PSCs as a promising alternative to their Pb-based counterparts. Figure 1 illustrates several factors contributing to V_{OC} deficits. We systematically summarize the challenges and strategies for enhancing Sn-based PSCs, categorizing the main content into four sections: morphology optimization, antioxidation doping, interface passivation, and energy level regulation. Some strategies involve delaying crystal kinetic to improve film morphology, while others focus on inhibiting the oxidation of Sn^{2+} to reduce bulk and surface defect densities. Designing charge transport layers with better-matched energy levels can minimize carrier losses at the interface, ultimately effectively enhancing the V_{OC} of the devices. We believe that this work can provide more systematic information on the material science and defect mechanisms of Sn-based perovskites, thereby aiding in the theoretical guidance for improving the performance of Sn-based PSCs.

2. Overview of the origin of V_{OC} deficits in Sn-based PSCs

2.1. Uncontrollable crystal kinetics growth and poor film morphology

The electron configuration of Pb^{2+} is [Xe]4 $f^{14}5d^{10}6s^2$, whereas the electron configuration of Sn^{2+} is [Kr]$4d^{10}5s^2$. Due to the absence of 4f orbitals in Sn^{2+}, the attraction from the nucleus to the 5s electrons is weaker. Consequently, Sn^{2+} is easily oxidized and exhibits strong Lewis acidity [37]. In the preparation of Pb-based perovskite films, high-temperature annealing is typically required to complete the phase transition. This step provides ample time for crystal growth, facilitating the formation of uniform and smooth perovskite films [38]. Conversely, in Sn-based perovskite films, the reaction of SnI_2 with Lewis basic ammonium salts such as CH_3NH_3I (MAI) and $HC(NH_2)_2I$ (FAI) is very rapid. Upon anti-solvent dripping, the perovskite film quickly transitions to the black perovskite phase without annealing [39]. This rapid crystallization process can result in an imbalance between nucleation and growth rates, leading to numerous three-dimensional defects such as voids, cracks and grain boundaries [40, 41]. Due to poor crystallinity and orientation, these three-dimensional defects hinder the effective extraction and collection of photogenerated charge carriers in the

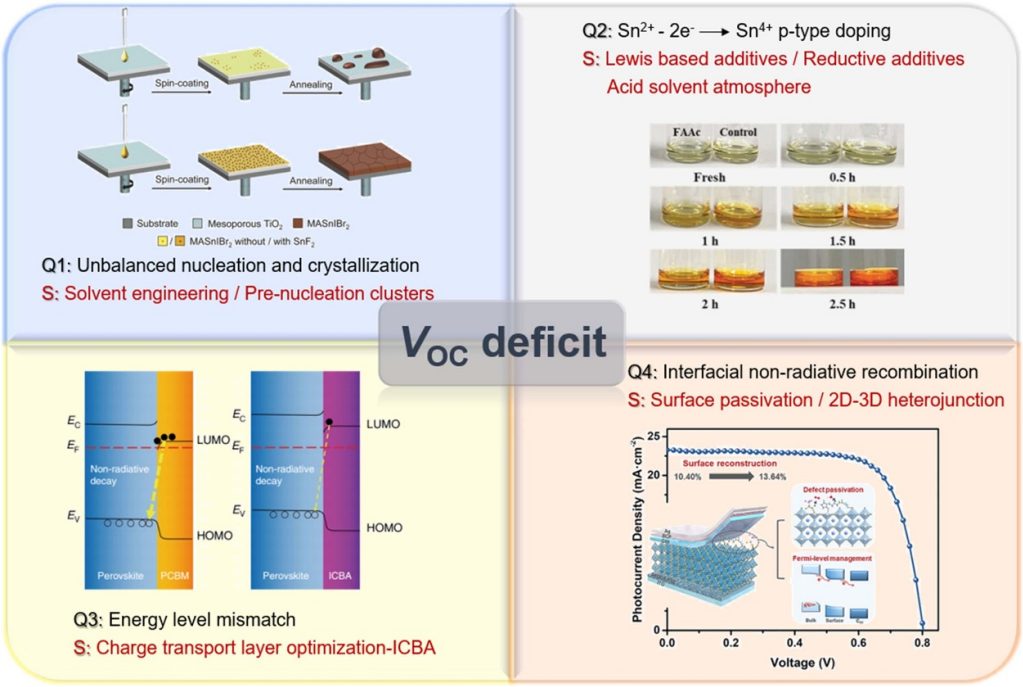

Figure 1. Schematic diagram of the reasons and strategies for V_{OC} deficit. Q1: [34] John Wiley & Sons. [Copyright © 2018 WILEY-VCH Verlag GmbH & Co. KGaA, Weinheim]. Q2: [35] John Wiley & Sons. [Copyright © 2023 WILEY-VCH Verlag GmbH & Co. KGaA, Weinheim]. Q3: Reproduced from [24]. CC BY 4.0. Q4: Reprinted with permission from [36]. Copyright (2022) American Chemical Society.

perovskite film [42]. Moreover, these defects are more susceptible to corrosion by oxygen and moisture, further declining device performance and stability [43]. Stress and strain caused by uncontrolled crystal growth can affect the electronic structure and the dynamics of charge carriers, further impacting V_{OC} [44]. Furthermore, uncontrollable crystal growth often introduces numerous point defects, such as vacancies, interstitials, and antisites [45]. These defects can act as recombination centers for charge carriers, increasing non-radiative recombination and consequently reducing V_{OC} [46]. To address these issues, researchers have been developing various strategies to modulate crystallization kinetics [47], passivate surface defects [48], and optimize fabrication processes [39] to enhance the quality of Sn-based perovskite films and the overall performance of PSCs.

Solution engineering is one of the most efficient and common methods for fabricating polycrystalline films. The choice of solvent and antisolvent has been found to be crucial to achieving high-quality Sn-based perovskite films *via* solution methods [49, 50]. During the one-step method, $ASnX_3$ perovskite is typically dissolved in dimethyl sulfoxide (DMSO) or n, n-dimethylformamide (DMF). Hao *et al* discovered that compared to other highly polar solvents such as DMF and N-methyl-2-pyrrolidone (NMP), SnI_2 can form an intermediate $SnI_2$3DMSO complex with the stronger coordinating solvent DMSO (figure 2(a)), allowing the organic cations to dissolve in the mother liquor and delaying crystallization [41]. DMSO is known for its strong coordination with Sn^{2+}, which can regulate the crystal kinetics of perovskite, resulting in uniform and dense perovskite films. However, the sulfoxide group (–S(=O)–CH_3) presents in DMSO can oxidize Sn^{2+} to Sn^{4+} [51]. Therefore, exploring or screening alternative solvents that can replace DMSO is also a viable strategy to mitigate this oxidation effect. Subsequently, Rao *et al* found that the larger-molecule volume of hexamethylphosphoramide (HMPA) exhibits stronger binding energy with SnI_2 (−0.595 eV vs −0.118 eV for $SnI_2$2DMSO), leading to the solvation structure of SnI_2 shifting from clustered coordination to monodisperse adducts (figure 2(b)). This transition promotes the uniformity of nucleation sites and extends the crystal growth process [52].

Various antisolvents have also been developed and applied in fabricating dense and uniform perovskite films. Commonly used antisolvents include diethyl ether (DE), toluene (TU), and chlorobenzene (CB), as they are effective in quickly extracting precursor solvents and obtaining high-quality Sn-based perovskite films [54]. A large number of pinholes were found in the perovskite films treated with DE. The perovskite films prepared using TU as an antisolvent exhibit a larger average grain size compared to those prepared with DE and CB; however, they also have a significant number of pinholes [43]. CB is the most commonly used antisolvent in the fabrication of Sn-based perovskite films, contributing to the formation of uniform and compact layers. The specific reason for this is that chlorobenzene has a high boiling point of 131 °C, which slows down the evaporation rate during the thermal annealing process, thereby extending the time for crystal growth. The presence of the solvent also provides sufficient

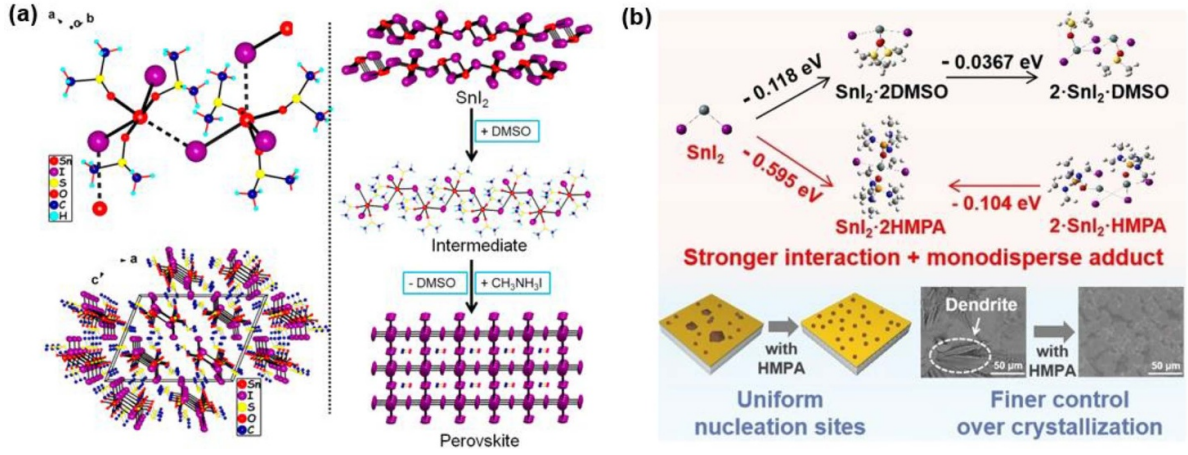

Figure 2. (a) Crystal structure of $SnI_2 \cdot 3DMSO$, an intermediate compound in the $CH_3NH_3SnI_3$ film fabrication process. Reprinted with permission from [41]. Copyright (2015) American Chemical Society. (b) Schematic diagram of the effect of hexamethylphosphoramide (HMPA) on dispersion of edge-sharing SnI_2 nanocrystals and regulation of crystallization kinetics. Top: SnI_2 clusters-induced uneven nucleation and rapid crystallization lead to poor-oriented film. Bottom: monodisperse SnI_2-HMPA adduct-induced uniform nucleation and a slow crystallization process in balance with it result in high-oriented film. [52] John Wiley & Sons. [Copyright © 2023 WILEY-VCH Verlag GmbH & Co. KGaA, Weinheim].

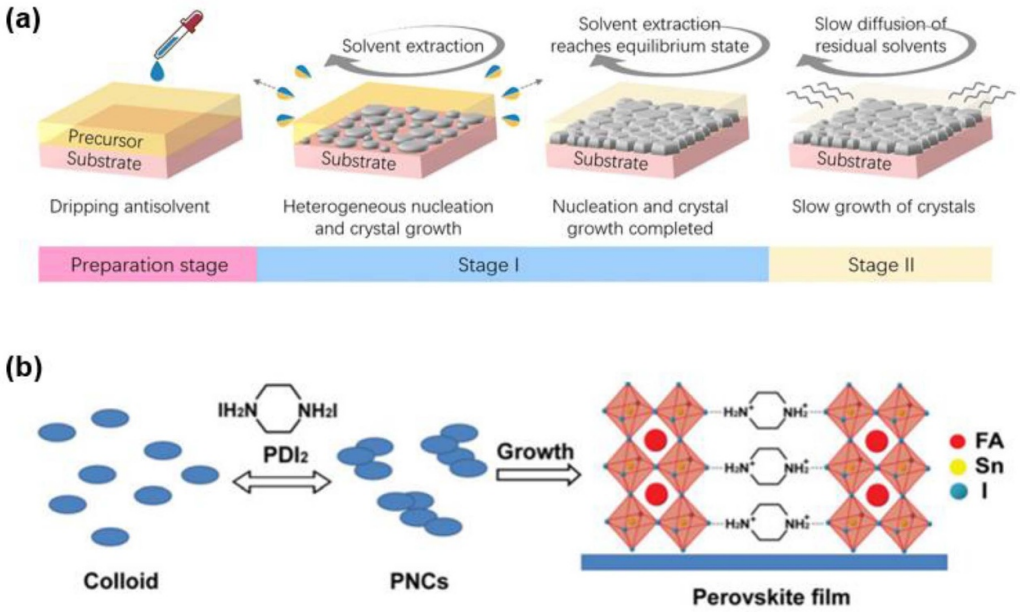

Figure 3. (a) Schematic diagram of Stage I and Stage II defined in time-driven steady-state absorption spectra. Reproduced from [23] with permission from the Royal Society of Chemistry. (b) Schematic illustration of the crystallization process of $FASnI_3$ perovskite films based on PNCs. [53]. John Wiley & Sons. [Copyright © 2020 WILEY-VCH Verlag GmbH & Co. KGaA, Weinheim].

flowability to the film, enabling adjacent nuclei to coalesce into larger grains [42]. However, chlorobenzene is a toxic substance, and long-term exposure may cause serious health effects. Zhang *et al* substituted the traditional toxic CB with a green antisolvent, diethyl carbonate (DEC), which retards the kinetics of solvent-antisolvent interaction (figure 3(a)). The resulting Sn-based perovskite film exhibits a gradient distribution of p-type self-doping from the top surface to the bottom surface, with reduced p-type self-doping at the top surface. The gradient in the energy band structure of the perovskite film improves the interfacial energy level alignment and generates an additional built-in electric field. This field provides a stronger driving force for charge separation, promotes charge transport, and effectively alleviates the accumulation of reverse charges at both interfaces [23]. The perovskite precursor could be regarded as a colloidal dispersion rather than a conventional solution [55]. Meng *et al* manipulated the chemical properties of $FASnI_3$ colloids by adding piperazine dihydriodide ($PDAI_2$). This facilitated the formation of stable pre-nucleation clusters (PNCs) as intermediate phases, thereby reducing the nucleation barrier of perovskites and yielding highly oriented Sn-based perovskite crystals (figure 3(b)) [53].

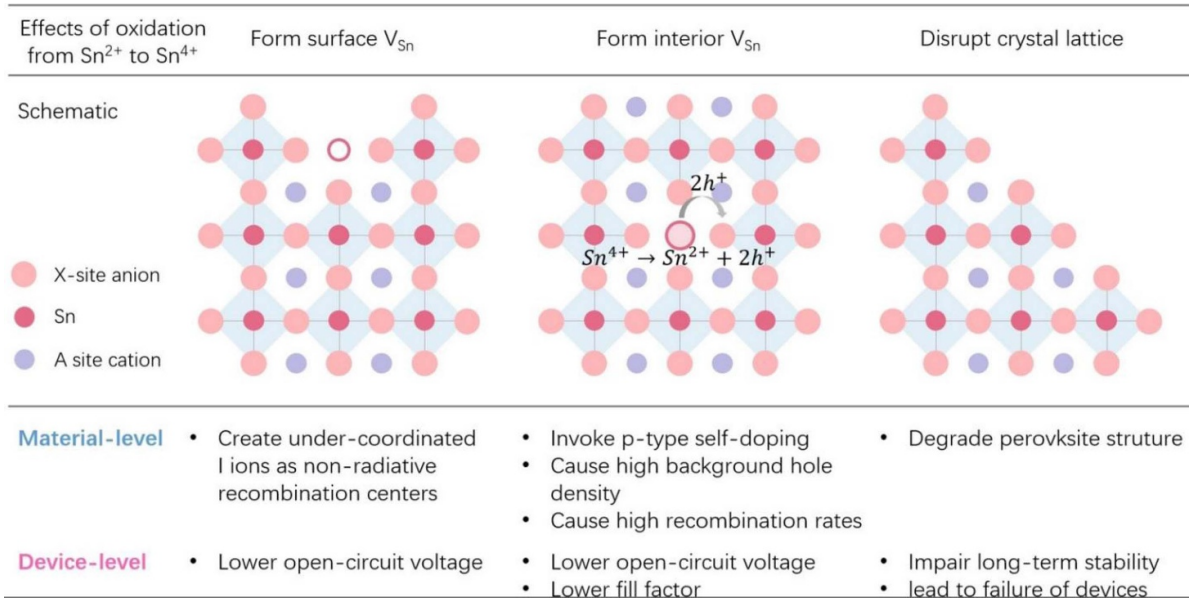

Figure 4. Effects of oxidation from Sn^{2+} to Sn^{4+} in Sn-based perovskites on material-level and device-level with schematic illustration. [48] John Wiley & Sons. [Copyright © 2023 WILEY-VCH Verlag GmbH & Co. KGaA, Weinheim].

2.2. High concentration of V_{Sn} defects due to the active ns^2 electrons of Sn^{2+}

Compared to Pb^{2+}, Sn^{2+} is more prone to oxidation to Sn^{4+} due to its standard redox potential of +0.15 V for the Sn^{2+}/Sn^{4+} couple, whereas the standard redox potential for the Pb^{2+}/Pb^{4+} couple is significantly higher at +1.67 V [49]. Furthermore, the electrons in the 6s orbitals of Pb exhibit an inert pair effect derived from the contraction of the lanthanides, an effect absent in Sn [56, 57]. The $5s^2$ electrons of Sn^{2+} are highly active, making Sn^{2+} easily oxidized to Sn^{4+} [58]. This oxidation reaction generates Sn vacancies (V_{Sn}) in the perovskite lattice, leading to the formation of shallow energy level defects near the valence band with low formation energies [59]. Sn^{4+} at the surface primarily acts as a non-radiative recombination center, capturing electrons and holes and inhibiting their thermal escape, leading to their annihilation with opposite charge carriers [60]. This process results in severe V_{OC} deficits, ultimately impairing the performance of photovoltaic devices [22]. Additionally, Sn^{4+} within the perovskite lattice spontaneously converts back to Sn^{2+}, releasing two holes into the valence band and inducing p-type self-doping in the perovskite (figure 4) [60]. This heavy p-type self-doping results in high intrinsic carrier concentrations (10^{17}–10^{19} cm^{-3}) [61]. The formation of both surface and internal V_{Sn} promotes lattice degradation, impairing the stability of Sn-based perovskites, and ultimately leading to the degradation of Sn-based PSCs [62].

Considering that perovskites are prepared based on Lewis acid-base adducts, with SnI_2 being a highly reactive Lewis acid. Lewis base additives can act as electron donors, passivating positively charged defects such as uncoordinated Sn^{2+} [13]. Tai *et al* introduced both hydroquinone sulfonic acid (KHQSA) and $SnCl_2$ into $FASnI_3$ perovskite films (figure 5(a)). The interaction between the sulfonic acid ($–SO_3$) group and Sn^{2+} ions resulted in the in-situ encapsulation of perovskite particles by the $SnCl_2$ additive complexation layer, significantly enhancing the oxidative stability of the perovskite film [63]. Lin *et al* introduced 8-hydroxyquinoline (8-HQ) into $FASnI_3$ films, where the N and O bidentate atoms can simultaneously coordinate with Sn^{2+}, forming a more stable complex (figure 5(b)) [64]. Lewis basic molecules typically contain one or more electron-donating functional groups that interact with Sn^{2+}, inhibiting its oxidation. To enhance the interaction between Lewis basic additives and Sn^{2+}, additives with multiple electron-donating functional groups can be selected. Liu *et al* incorporated melamine into Sn-based perovskites, where multiple functional groups such as –C=N and $–NH_2$ (figure 5(c)) can passivate Sn^{2+} through Lewis acid-base adduction and hydrogen bonding [65]. Ma *et al* incorporated α-Tocopherol into the $FASnI_3$ perovskite [39]. It forms van der Waals and hydrogen bond interactions with the formamidine ion (FA^+) and the $[SnI_6]^{4-}$ octahedron at the perovskite terminals. By passivating with α-Tocopherol, both surface and interior oxidation of the perovskite are significantly suppressed, as α-Tocopherol firmly embeds itself on the perovskite surface (figure 5(d)).

Even industrially synthesized SnI_2 inevitably contains Sn^{4+} impurities. Zeng *et al* proposed a convenient solution method for purifying SnI_2 in Sn-based PSCs, which involves using toluene as a solvent to dissolve the undesired SnI_4, while retaining the SnI_2 source [67]. Gu *et al* added Sn powder to the precursor solution and obtained a high-purity $FASnI_3$ precursor solution after 5 h of heating and stirring [68]. Nakamura

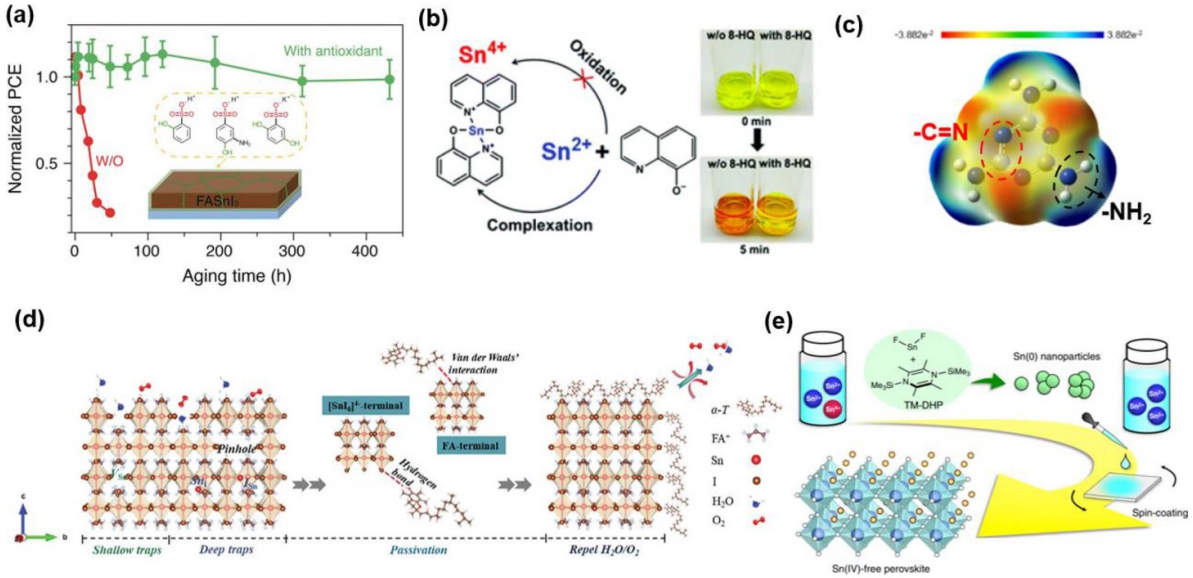

Figure 5. (a) Sn-based PSCs with significantly improved stability to oxidation were prepared by introducing hydroxybenzene sulfonic acid or a salt thereof as an antioxidant additive into the perovskite precursor solution. [63] John Wiley & Sons. [Copyright © 2019 WILEY-VCH Verlag GmbH & Co. KGaA, Weinheim]. (b) Schematic diagram of the molecular structure of the 8-HQ bidentate ligand and the complexation with Sn^{2+}. Reproduced from [64] with permission from the Royal Society of Chemistry. (c) The molecular electrostatic potential of melamine. The –C=N functional group is circled by a red dashed line, and the $–NH_2$ functional group is circled by a black dashed line. Reprinted from [65], Copyright (2023), with permission from Elsevier. (d) Schematic illustration of defect profile in pristine Sn perovskite film with a variety of Sn or I-related defects, and corresponding passivation strategy caused by hydrogen bonding and van der Waals interactions between perovskite and α-Tocopherol. [39] John Wiley & Sons. [Copyright © 2024 WILEY-VCH Verlag GmbH & Co. KGaA, Weinheim]. (e) Schematic illustration of the Sn^{4+} scavenging method. Reproduced from [66]. CC BY 4.0.

et al observed that the derivative of dihydropyridine (TM-DHP) could react with SnF_2 already present in the precursor solution to produce Sn nanoparticles (figure 5(e)). These Sn nanoparticles reduce Sn^{4+} to Sn^{2+} through a comproportionation reaction ($Sn(s) + Sn^{4+} \rightarrow 2Sn^{2+}$), thereby eliminating Sn^{4+} impurities from $FA_{0.75}MA_{0.25}SnI_3$ perovskite [66]. Hydrazine-based additives have also been shown to effectively reduce excess Sn^{4+} in perovskite films. In 2016, Song *et al* established a vapor atmosphere of hydrazine (N_2H_4) to mitigate the formation of Sn^{4+} during the spin-coating process of perovskite films [69]. Wang *et al* introduced phenylhydrazine hydrochloride (PHCl, PHCl-Br) into $FASnI_3$ perovskite films. With its reducing hydrazine group and hydrophobic phenyl group, PH^+ can diminish existing Sn^{4+} and prevent further oxidation of $FASnI_3$ [70, 71].

During the preparation of perovskite films, solid-state additives may undergo phase separation, resulting in decreased crystallinity of the perovskite and the formation of charge recombination centers, thereby impeding charge transport. In contrast, liquid acid additives not only stabilize Sn^{2+}, but also do not induce phase separation. An acidic atmosphere has been proved to inhibit the spontaneous oxidation of Sn^{2+} [72, 73]. Meng *et al* utilized liquid formic acid (LFA) as a 50% solvent. Upon annealing, it completely evaporates without residue, ultimately yielding $FASnI_3$ perovskite thin films with low electron trap density and high crystallinity [74]. Su *et al* discovered that the addition of acetic acid (HAc) into the precursor solution could lower the supersaturation concentration, forming prenucleation clusters while delaying crystallization and inhibiting the oxidation of Sn^{2+} [75].

2.3. Interfacial non-radiative recombination

Within the perovskite or interfacial transport layers of PSCs, band tails or energy disorder can create electronic states that lead to non-radiative recombination [72]. To mitigate carrier recombination, interfacial passivation through post-treatment has proven effective. This commonly involves covering the surface of three-dimensional perovskite with a two-dimensional perovskite layer that acts both as a passivation layer, reducing surface cation and anion defects through hydrogen or ionic bonding, and as a hydrophobic encapsulation layer. This dual function minimizes non-radiative recombination and enhances device efficiency, while also protecting the underlying three-dimensional structure and improving device stability [76].

Wei *et al* introduced phenethylamine (PEA) ligands into the anti-solvent to prepare mixed Sn-Pb perovskite films (figure 6(a)), where perovskite particles were anchored by ultra-thin two-dimensional perovskite to overcome efficiency-stability decay [73]. Subsequently, Liao *et al* dissolved phenethylammonium bromide (PEABr) in isopropanol (IPA) and spin-coated it onto $FASnI_3$ films, forming a low-dimensional layer on the surface to passivate surface defects of the perovskite films (figure 6(b)) [77]. Wu *et al* treated annealed $FASnI_3$ films with 4-(trifluoromethyl)benzylammonium

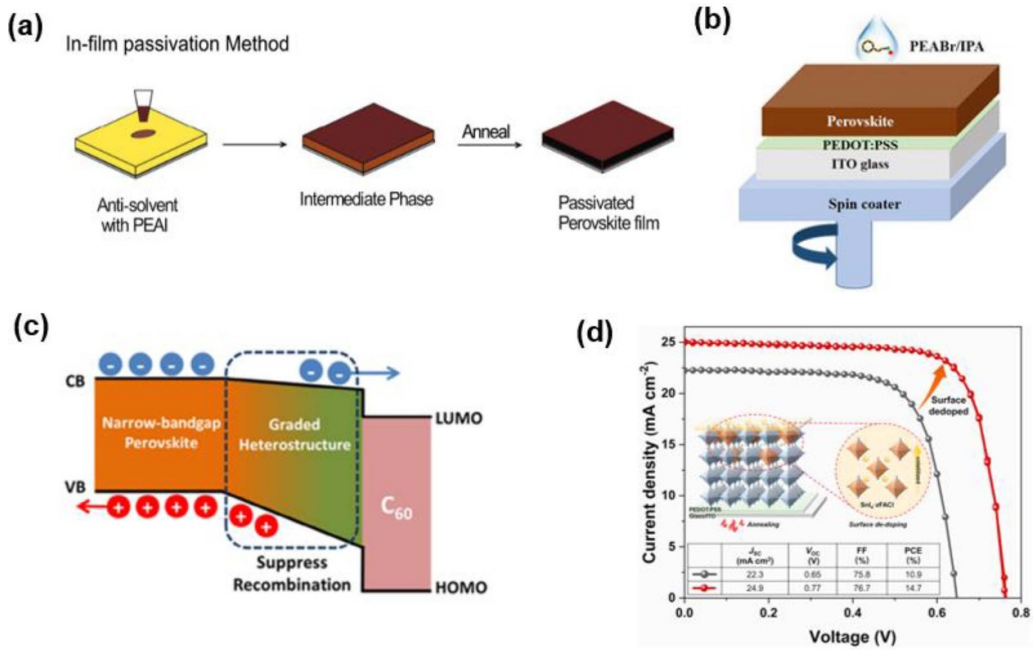

Figure 6. (a) Schematic diagram of processing method to achieve in-film passivation. [73] John Wiley & Sons. [Copyright © 2020 WILEY-VCH Verlag GmbH & Co. KGaA, Weinheim]. (b) Schematic illustration of PEABr treatment. [77] John Wiley & Sons. [Copyright © 2019 WILEY-VCH Verlag GmbH & Co. KGaA, Weinheim]. (c) Diagram of energy level alignment at the perovskite/C_{60} interface. [78] John Wiley & Sons. [Copyright © 2020 WILEY-VCH Verlag GmbH & Co. KGaA, Weinheim]. (d) A chemo-thermal dedoping process is therefore introduced to reduce the Sn(IV) self-dopants on the film surface. Reprinted from [19], Copyright (2022), with permission from Elsevier.

($TFBA^+$) dissolved in chloroform [78]. The cation exchange between $FASnI_3$ and $TFBA^+$ facilitates the construction of a heterojunction structure at the perovskite/C_{60} interface, selectively extracting photo-generated carriers and serving as an energy barrier to suppress Sn^{2+} oxidation (figure 6(c)). Ultimately, they successfully increased the V_{OC} by 120 meV, achieving a PCE of 10.96% and a V_{OC} of 0.70 V. In another study, Nishimura *et al* dissolved ethylenediamine (EDA) in toluene, directly spin-coating it on perovskite films, and fabricated an inverted structure device of FTO/PEDOT: PSS/$FA_{0.98}EDA_{0.01}Sn_{0.95}Ge_{0.05}I_3$/$C_{60}$/BCP/Ag/Au. Benefiting from the passivation effect of EDA, they successfully increased the device's V_{OC} from 0.70 V to 0.84 V and achieved a PCE of 13.24% [17]. However, even with the use of orthogonal solvents, post-treatment techniques may still corrode the underlying perovskite layer to some extent. Zhou *et al* introduced a chemo-thermal dedoping process, leveraging the complexation between FACl and Sn(IV) iodide components, to remove Sn(IV) during thermal annealing (figure 6(d)) [19].

2.4. Unmatched band level alignment

Another significant factor limiting the V_{OC} is the unmatched energy level alignment, which leads to an imbalance in charge transport [56]. Typically, photogenerated electrons should be selectively extracted by the electron transport layer (ETL), while photogenerated holes should be blocked from crossing the perovskite/ETL interface by a large Schottky barrier. Conversely, photogenerated holes should be selectively extracted by the hole transport layer (HTL) [79]. Imperfect charge transfer can result in carrier recombination losses at the interface. For instance, as the light intensity increases, the split of the quasi-Fermi level continues to increase, but the V_{OC} reaches saturation, possibly due to mismatches in charge-selective contacts [76, 80]. In Sn-based PSCs, this abnormal loss of V_{OC} due to mismatched energy levels is particularly severe (figure 7(a)).

In inverted Sn-based PSCs, the HTL at the bottom layer not only transports holes but also provides additional protection to the photoactive layer. Commonly used HTL materials include NiO_X [81], CuSCN [84], and poly(3,4-ethylenedioxythiophene) polystyrene sulfonate (PEDOT: PSS) [83]. Despite the stability advantages of fully inorganic materials such as NiO_X and CuSCN, they still encounter certain challenges. NiO_X contains multivalent Ni elements, surface oxygen vacancies, and uncoordinated metal ion defects [85]. Although CuSCN is a p-type semiconductor material, its hole mobility (0.1 $cm^2\ V^{-1}{\cdot}s^{-1}$) still lags behind the best-performing p-type semiconductors on the market. Additionally, the long-term development of CuSCN is restricted by the technology for preparing high-quality, controllable thin films [86].

PEDOT: PSS, as a conductive polymer, has been widely used in inverted Sn-based PSCs due to its excellent conductivity, good film-forming properties, and solution processability. However, given that the acidic nature of PEDOT: PSS may adversely affect the long-term stability, researchers are focused on modifying PEDOT: PSS to address this issue. Xu *et al* doped triisopropoxy vanadium oxide ($C_9H_{21}O_4V$) into the PEDOT: PSS solution. Following low-temperature heat

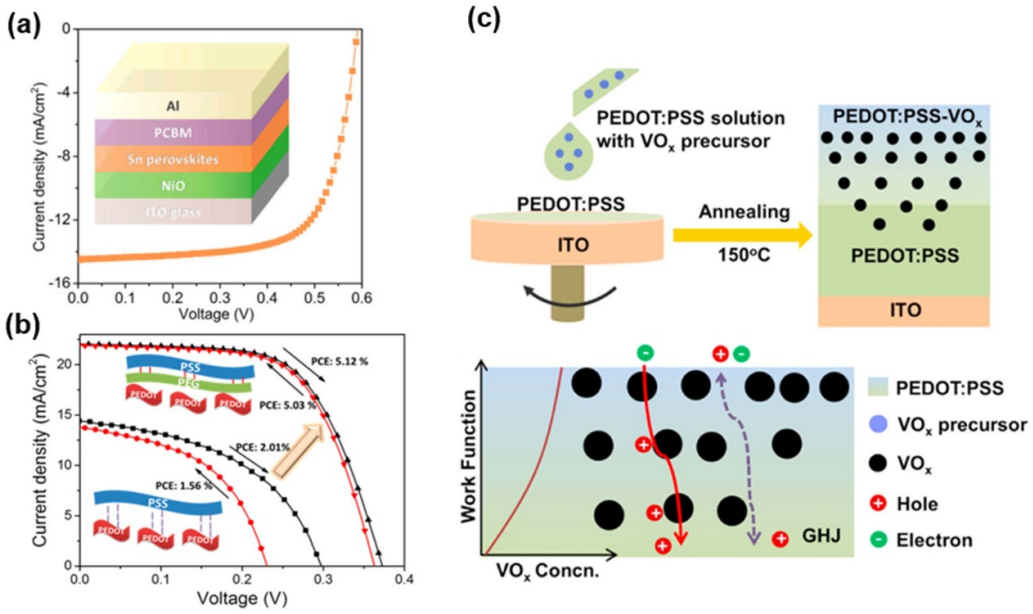

Figure 7. (a) Device architecture and current density–voltage (J–V) characteristics of the device. Reprinted with permission from [81]. Copyright (2017) American Chemical Society. (b) Schematic illustration of the charge transport dynamics and the work function of the HTL as a function of VO_x concentration in gradient heterojunction structure. Reprinted from [82], Copyright (2020), with permission from Elsevier. (c) Schematic diagram of PEG intercalating into PEDOT: PSS. Reprinted with permission from [83]. Copyright (2018) American Chemical Society.

treatment of the modified PEDOT: PSS film, high work function (W_F) vanadium oxide (VO_X) formed on the surface of the hole transport layer (HTL), which facilitated the formation of a gradient heterojunction (GHJ). This GHJ structure effectively lowered the energy barrier between the HTL and the perovskite layer, enhancing charge separation. Additionally, the surface of PEDOT: PSS exhibited increased hydrophobicity and reduced acidity, thereby improving the stability of the device (figure 7(b)) [82]. Liu *et al* discovered that the surface of PEDOT: PSS films is typically rich in PSS, and the surface dipoles result in a deeper W_F for PEDOT: PSS. After adding a small amount of polyethylene glycol (PEG) to PEDOT, the PEG forms hydrogen bonds with the SO_3H^+ groups in PSS, reducing the Coulomb interaction between PEDOT and PSS. As excess PSS separates, a PEDOT-rich region forms on the film surface, causing the surface dipoles to disappear and thus increasing the W_F of PEDOT: PSS. This change reduces the energy barrier for carrier transfer between $FASnI_3$ and PEDOT: PSS, significantly enhancing the photovoltaic performance of the device (figure 7(c)) [83].

Ideal ETLs need to possess high electron mobility, favorable hole blocking properties, and uniform coverage on the surface of perovskite films. Common ETLs include fullerene (C_{60}) and its derivatives ($PC_{61}BM$), and Indene-C_{60} bisadduct (ICBA) (figure 8(a)) [87]. In the early research of Sn-based PSCs, fullerene and its derivatives were widely used. Due to the weak binding energy of excitons, C_{60} and $PC_{61}BM$ primarily serve for charge extraction and transport. Additionally, Bathocuproine (BCP), with its deep highest occupied molecular orbital (HOMO) level, is also commonly used in conjunction with fullerene to form a composite layer that blocks the migration of holes to the electrode.

Considering the shallow conduction band level of Sn-based perovskite, it is essential to select an ETL with a shallower energy level to enhance the V_{OC}. $PC_{61}BM$ exhibits a larger bandgap shift due to its deeper band position. Jiang *et al* pointed out that the lowest unoccupied molecular orbital (LUMO) level of ICBA (−3.74 eV) is shallower than that of $PC_{61}BM$ (−3.91 eV), which is expected to boost the device's V_{OC} (figure 8(b)) [24]. By using ICBA as the ETL, researchers managed to improve the device's V_{OC} to 0.94 V, a significant improvement over devices employing $PC_{61}BM$ as the ETL (0.6 V). However, it has been observed that the J_{SC} is relatively low when using ICBA, and the specific reason for this remains unclear. Additionally, the high cost of ICBA is not conducive to large-scale production. In 2023, Yang *et al* designed and synthesized ETLs with higher LUMO levels, single-isomer C_{60}- and C_{70}-based diethylmalonate functionalized bisadducts ($C_{60}BB$, and $C_{70}BB$), greatly improving the device performance (figure 8(c)) [88]. To effectively mitigate the V_{OC} deficits of the device, further development of ETL with suitable energy level is crucial to minimize energy losses and suppress carrier recombination.

Through the above discussion, it is evident that non-radiative recombination resulting from surface defects and mismatched energy alignment at interfaces significantly impacts the V_{OC} and PCE of Sn-based PSCs. Accordingly, we have summarized the factors contributing to V_{OC} deficits and the strategies employed to address them, along with corresponding examples, in table 2.

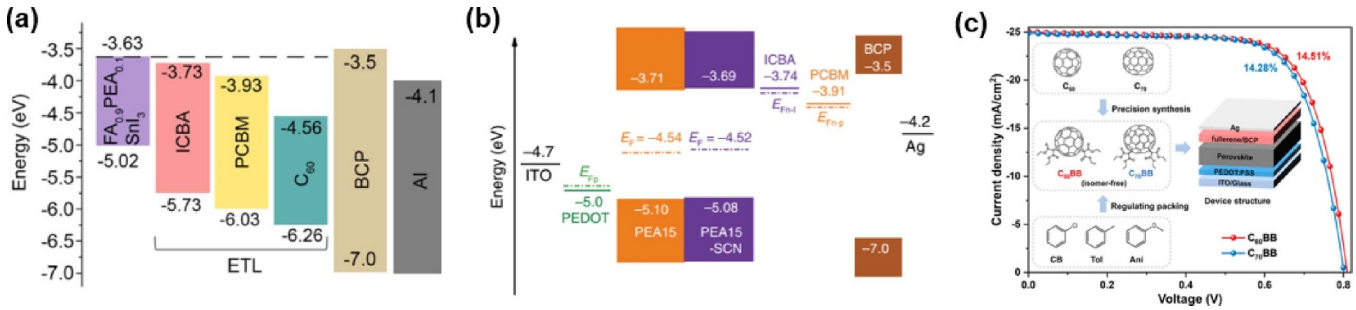

Figure 8. (a) Energy level diagram of PSCs using different ETL. Reprinted with permission from [87]. Copyright (2020) American Chemical Society. (b) Schematic illustration of energy levels. Dashed lines represent the quasi-Fermi level of ICBA (E_{Fn-I}), PCBM (E_{Fn-P}), and PEDOT (E_{Fp}). Reproduced from [24]. CC BY 4.0. (c) Synthesis route of C_{70}BB and C_{70}BB. Reprinted with permission from [88]. Copyright (2023) American Chemical Society.

Table 2. Summary of the reasons contributing to V_{OC} deficits and strategies used to mitigate them.

No.	Reason for V_{OC} deficits	Strategies
1	Uncontrolled Crystal Dynamics	(1) DMSO Complexation [41] (2) HMPA Binding [51] (3) Anti-Solvent Effects [42, 43] (4) Green Anti-Solvent [23] (5) Colloid Manipulation [53]
2	Spontaneous Oxidation of Sn^{2+}	(1) In-Situ Encapsulation [63, 64] (2) Surface Passivation [39] (3) SnI_2 purification [66–68] (4) Reductive Atmosphere [70, 71, 74, 75]
3	Interface Non-radiative Recombination Deficits	(1) Post-treatment [73, 77, 78] (2) Chemo-thermal Dedoping [19]
4	Unmatched Energy Level	(1) Modified PEDOT: PSS [82, 83] (2) Usage of ICBA [24] (3) Innovative ETL Synthesis [88]

3. Conclusions and perspectives

Sn-based PSCs with narrow bandgap can theoretically achieve high V_{OC}; however, in practice, they frequently encounter significant V_{OC} deficits, typically ranging from 0.4 to 0.6 V. This deficit primarily stems from the relatively high defect density in perovskite films prepared *via* solution processes, attributed to rapid crystallization and the inherent oxidation of Sn^{2+}. Defects on the surface and within the film typically serve as major recombination centers, capturing carriers and thus limiting carrier transport and collection. Hence, the V_{OC} is significantly affected by intrinsic crystal defects within the film, external defects (such as pinholes and grain boundaries), and interface defects between the ETL and the HTL.

To alleviate voltage deficits, it is crucial to employ effective methods that suppress carrier recombination at the perovskite film surface and enhance charge extraction efficiency at the heterojunction interface. Specific approaches, including enhancing the film preparation process through solvent engineering, additive engineering, and surface passivation, are aimed at creating highly dense, smooth, and nearly grain boundary-free perovskite films. Additionally, optimizing the device structure to minimize energy losses at the perovskite/transport layers is also crucial. By integrating these strategies, there is a significant potential to reduce V_{OC} deficits and thereby enhance the overall performance of Sn-based PSCs.

Future research should focus on reducing defect density to optimize both the single perovskite crystal and the interfacial transport layer. High-efficiency Sn-based PSCs primarily employ the FA/PEA mixed composition, with a device structure of ITO/PEDOT: PSS/Perovskite/ICBA/BCP/Ag. Experimental observations indicate that devices using ICBA as the ETL often exhibit lower J_{SC}, but the reasons for this phenomenon remain unclear. Enhancing the photocurrent of devices while utilizing ICBA could potentially lead to further breakthroughs in the PCEs of Sn-based PSCs. Moreover, the high cost of ICBA adds to the experimental expenses. Hence, it is crucial to develop novel ETL materials with low cost, matched energy levels, and excellent conductivity. Ultimately,

Sn-based PSCs have achieved high efficiency up to 15.7% [33], however, there still exists discrepancy in both efficiency and stability compared to Pb-based PSCs. To advance the commercialization of Sn-based PSCs, we must not only focus on improving device efficiency but also fundamentally address tin oxidation to ensure stability while pursuing high efficiency.

Data availability statement

All data that support the findings of this study are included within the article (and any supplementary files).

Acknowledgments

This work was supported by National Natural Science Foundation of China (NSFC 51972137 and 62321166653), the Innovative Capacity Building Foundation of Jilin Province Development and Reform Commission (2023C034-5), and the Science and Technology Planning Project of Jilin Province (20230101020JC).

ORCID iD

Ning Wang https://orcid.org/0000-0001-9570-952X

References

[1] Lee J-W, Seol D-J, Cho A-N and Park N-G 2014 High-efficiency perovskite solar cells based on the black polymorph of $HC(NH_2)_2PbI_3$ *Adv. Mater.* **26** 4991–8
[2] Deng J, Yuan S, Xiong H, Ma Z, Wu W, Wang M, Lou Z, Fan J and Li W 2023 Br-I ordered $CsPbBr_2I$ perovskite single crystal toward extremely high mobility *Chem* **9** 1929–44
[3] Xing G, Mathews N, Sun S, Lim S S, Lam Y M, Grätzel M, Mhaisalkar S and Sum T C 2013 Long-range balanced electron- and hole-transport lengths in organic-inorganic $CH_3NH_3PbI_3$ *Science* **342** 344–7
[4] Liu X-K, Xu W, Bai S, Jin Y, Wang J, Friend R H and Gao F 2021 Metal halide perovskites for light-emitting diodes *Nat. Mater.* **20** 10–21
[5] Wang Z *et al* 2023 Suppressed phase segregation for triple-junction perovskite solar cells *Nature* **618** 74–79
[6] Kazim S, Nazeeruddin M K, Grätzel M and Ahmad S 2014 Perowskit als lichtabsorptionsmaterial: ein durchbruch in der photovoltaik *Angew. Chem.* **126** 2854–67
[7] Gao P, Grätzel M and Nazeeruddin M K 2014 Organohalide lead perovskites for photovoltaic applications *Energy Environ. Sci.* **7** 2448–63
[8] Stranks S D, Nayak P K, Zhang W, Stergiopoulos T and Snaith H J 2015 Formation of thin films of organic–inorganic perovskites for high-efficiency solar cells *Angew. Chem., Int. Ed.* **54** 3240–8
[9] Liang L and Gao P 2018 Lead-free hybrid perovskite absorbers for viable application: can we eat the cake and have it too? *Adv. Sci.* **5** 1700331
[10] Fu Q, Tang X, Huang B, Hu T, Tan L, Chen L and Chen Y 2018 Recent progress on the long-term stability of perovskite solar cells *Adv. Sci.* **5** 1700387
[11] Kojima A, Teshima K, Shirai Y and Miyasaka T 2009 Organometal halide perovskites as visible-light sensitizers for photovoltaic cells *J. Am. Chem. Soc.* **131** 6050–1
[12] Liang Z, Zhang Y, Xu H, Chen W, Liu B, Zhang J, Zhang H, Wang Z, Kang D-H and Zeng J 2023 Homogenizing out-of-plane cation composition in perovskite solar cells *Nature* **624** 557–63
[13] Han D, Wang J, Agosta L, Zang Z, Zhao B, Kong L, Lu H, Mosquera-Lois I, Carnevali V and Dong J 2023 Tautomeric mixture coordination enables efficient lead-free perovskite LEDs *Nature* **622** 493–8
[14] Tai Q, Cao J, Wang T and Yan F 2019 Recent advances toward efficient and stable Tin-based perovskite solar cells *EcoMat* **1** e12004
[15] Diau E W-G, Jokar E and Rameez M 2019 Strategies to improve performance and stability for Tin-based perovskite solar cells *ACS Energy Lett.* **4** 1930–7
[16] Guillemoles J-F, Kirchartz T, Cahen D and Rau U 2019 Guide for the perplexed to the Shockley–Queisser model for solar cells *Nat. Photon.* **13** 501–5
[17] Nishimura K, Kamarudin M A, Hirotani D, Hamada K, Shen Q, Iikubo S, Minemoto T, Yoshino K and Hayase S 2020 Lead-free tin-halide perovskite solar cells with 13% efficiency *Nano Energy* **74** 104858
[18] Li B *et al* 2022 Efficient and stable Tin perovskite solar cells by pyridine-functionalized fullerene with reduced interfacial energy loss *Adv. Funct. Mater.* **32** 2205870
[19] Zhou J, Hao M, Zhang Y, Ma X, Dong J, Lu F, Wang J, Wang N and Zhou Y 2022 Chemo-thermal surface dedoping for high-performance tin perovskite solar cells *Matter* **5** 683–93
[20] Zhang Y, Zhao B, Liu L, Zhou J, Ma X and Wang N 2024 Efficient Tin perovskite solar cells via suppressing autoxidation in inert atmosphere *Small* **20** 2306115
[21] Zhang Y, Zhao B, Liu L and Wang N 2023 Interfacial molecular lock enables highly efficient Tin perovskite solar cells *ACS Appl. Mater. Interfaces* **15** 53362–70
[22] Jiang Y *et al* 2022 Dual-site passivation of tin-related defects enabling efficient lead-free tin perovskite solar cells *Nano Energy* **103** 107818
[23] Zhang Z *et al* 2023 Green-antisolvent-regulated distribution of p-type self-doping enables tin perovskite solar cells with an efficiency of over 14% *Energy Environ. Sci.* **16** 3430–40
[24] Jiang X *et al* 2020 Ultra-high open-circuit voltage of tin perovskite solar cells via an electron transporting layer design *Nat. Commun.* **11** 1245
[25] Li T, Zhang Z, He F, Deng L, Yang Y, Mo X, Zhan Y and Liang J 2023 Alleviating the crystallization dynamics and suppressing the oxidation process for tin-based perovskite solar cells with fill factors exceeding 80 percent *Adv. Funct. Mater.* **33** 2308457
[26] Liu G *et al* 2022 Multidentate chelation heals structural imperfections for minimized recombination loss in lead-free perovskite solar cells *Angew. Chem., Int. Ed.* **61** e202209464
[27] Jiang X *et al* 2021 One-step synthesis of $SnI_2{\cdot}(DMSO)_x$ adducts for high-performance tin perovskite solar cells *J. Am. Chem. Soc.* **143** 10970–6
[28] Zhu Z, Jiang X, Yu D, Yu N, Ning Z and Mi Q 2022 Smooth and compact $FASnI_3$ films for lead-free perovskite solar cells with over 14% efficiency *ACS Energy Lett.* **7** 2079–83
[29] Yu -B-B, Chen Z, Zhu Y, Wang Y, Han B, Chen G, Zhang X, Du Z and He Z 2021 Heterogeneous 2D/3D Tin-halides perovskite solar cells with certified conversion efficiency breaking 14% *Adv. Mater.* **33** 2102055
[30] Liu G, Jiang X, Feng W, Yang G, Chen X, Ning Z and Wu W-Q 2023 Synergic electron and defect compensation minimizes voltage loss in lead-free perovskite solar cells *Angew. Chem., Int. Ed.* **62** e202305551

[31] Sun C *et al* 2023 Well-defined fullerene bisadducts enable high-performance Tin-based perovskite solar cells *Adv. Mater.* **35** 2205603

[32] Chen J *et al* 2024 Efficient Tin-based perovskite solar cells with trans-isomeric fulleropyrrolidine additives *Nat. Photon.* **18** 464–70

[33] Shi Y, Zhu Z, Miao D, Ding Y and Mi Q 2024 Interfacial dipoles boost open-circuit voltage of tin halide perovskite solar cells *ACS Energy Lett.* **9** 1895–7

[34] Xiao M, Gu S, Zhu P, Tang M, Zhu W, Lin R, Chen C, Xu W, Yu T and Zhu J 2018 Tin-based perovskite with improved coverage and crystallinity through Tin-fluoride-assisted heterogeneous nucleation *Adv. Opt. Mater.* **6** 1700615

[35] Wang S, Yao H, Zhu W, Wu C, Tang Z, Liu J, Ding L and Hao F 2023 Stabilization of perovskite lattice and suppression of Sn^{2+}/Sn^{4+} oxidation via formamidine acetate for high efficiency Tin perovskite solar cells *Adv. Funct. Mater.* **33** 2215041

[36] Li H, Chang B, Wang L, Wang Z, Pan L, Wu Y, Liu Z and Yin L 2022 Surface reconstruction for Tin-based perovskite solar cells *ACS Energy Lett.* **7** 3889–99

[37] Zhang J and Zhong Y 2022 Origins of p-doping and nonradiative recombination in $CsSnI_3$ *Angew. Chem.* **134** e202212002

[38] Li T, He F, Liang J and Qi Y 2023 Functional layers in efficient and stable inverted tin-based perovskite solar cells *Joule* **7** 1966–91

[39] Ma X, Zhang Y, Zhou J, Liu L, Ju M and Wang N 2024 Mitigating surface defects in Tin-based perovskite films with α-tocopherol for enhanced photovoltaic performance *Small* **20** 2307373

[40] Yuan F *et al* 2020 Color-pure red light-emitting diodes based on two-dimensional lead-free perovskites *Sci. Adv.* **6** eabb0253

[41] Hao F, Stoumpos C C, Guo P, Zhou N, Marks T J, Chang R P and Kanatzidis M G 2015 Solvent-mediated crystallization of $CH_3NH_3SnI_3$ films for heterojunction depleted perovskite solar cells *J. Am. Chem. Soc.* **137** 11445–52

[42] Liu X, Yan K, Tan D, Liang X, Zhang H and Huang W 2018 Solvent engineering improves efficiency of lead-free Tin-based hybrid perovskite solar cells beyond 9% *ACS Energy Lett.* **3** 2701–7

[43] Ji L, Zhang T, Wang Y, Zhang P, Liu D, Chen Z and Li S 2017 Realizing full coverage of stable perovskite film by modified anti-solvent process *Nanoscale Res. Lett.* **12** 367

[44] Andrei F, Dinescu M, Ion V, Craciun F, Birjega R and Scarisoreanu N D 2023 Impact of structural strain in perovskite epitaxial thin films on their functional properties *Crystals* **13** 1686

[45] Cui G, Zhang X, Zhu Y, Chen C, Gao Z, Wang J, Xie G, Huang H, Zou B and Zhao D 2023 Reduced open-circuit voltage deficit in wide-bandgap perovskite solar cells enabled by thiazolidine-based interfacial engineering *J. Mater. Chem.* C **11** 10259–65

[46] Pappenberger R, Diercks A, Petry J, Moghadamzadeh S, Fassl P and Paetzold U W 2024 Bandgap engineering of two-step processed perovskite top cells for perovskite-based tandem photovoltaics *Adv. Funct. Mater.* **34** 2311424

[47] Li M, Li F, Gong J, Zhang T, Gao F, Zhang W-H and Liu M 2022 Advances in Tin(II)-based perovskite solar cells: from material physics to device performance *Small Struct.* **3** 2100102

[48] Zhang Z, Huang Y, Jin J, Jiang Y, Xu Y, Zhu J and Zhao D 2023 Mechanistic understanding of oxidation of Tin-based perovskite solar cells and mitigation strategies *Angew. Chem., Int. Ed.* **62** e202308093

[49] Aftab A and Ahmad M I 2021 A review of stability and progress in Tin halide perovskite solar cell *Sol. Energy* **216** 26–47

[50] Dong H, Ran C, Gao W, Sun N, Liu X, Xia Y, Chen Y and Huang W 2022 Crystallization dynamics of Sn-based perovskite thin films: toward efficient and stable photovoltaic devices *Adv. Energy Mater.* **12** 2102213

[51] Abate A 2023 Stable Tin-based perovskite solar cells *ACS Energy Lett.* **8** 1896–9

[52] Rao H, Su Y, Liu G L, Zhou H B, Yang J, Sheng W P, Zhong Y, Tan L C and Chen Y W 2023 Monodisperse adducts-induced homogeneous nucleation towards high-quality Tin-based perovskite film *Angew. Chem., Int. Ed.* **62** e202306712

[53] Meng X, Li Y, Qu Y, Chen H, Jiang N, Li M, Xue D J, Hu J S, Huang H and Yang S 2020 Crystallization kinetics modulation of $FASnI_3$ films with pre-nucleation clusters for efficient lead-free perovskite solar cells *Angew. Chem., Int. Ed.* **60** 3693–8

[54] Cao K, Cheng Y, Chen J, Huang Y, Ge M, Qian J, Liu L, Feng J, Chen S and Huang W 2020 Regulated crystallization of $FASnI_3$ films through seeded growth process for efficient tin perovskite solar cells *ACS Appl. Mater. Interfaces* **12** 41454–63

[55] Ran C, Gao W, Li N, Xia Y, Li Q, Wu Z, Zhou H, Chen Y, Wang M and Huang W 2019 Facet-dependent control of PbI_2 Colloids for over 20% efficient perovskite solar cells *ACS Energy Lett.* **4** 358–67

[56] Xiang J, Wang K, Xiang B and Cui X 2018 Sn^{2+}-stabilization in $MASnI_3$ perovskites by superhalide incorporation *J. Chem. Phys.* **148** 124111

[57] Giorgi G, Fujisawa J-I, Segawa H and Yamashita K 2013 Small photocarrier effective masses featuring ambipolar transport in methylammonium lead iodide perovskite: a density functional analysis *J. Phys. Chem. Lett.* **4** 4213–6

[58] Wong A B, Bekenstein Y, Kang J, Kley C S, Kim D, Gibson N A, Zhang D, Yu Y, Leone S R and Wang L-W 2018 Strongly quantum confined colloidal cesium tin iodide perovskite nanoplates: lessons for reducing defect density and improving stability *Nano Lett.* **18** 2060–6

[59] Noel N K, Stranks S D, Abate A, Wehrenfennig C, Guarnera S, Haghighirad A-A, Sadhanala A, Eperon G E, Pathak S K and Johnston M B 2014 Lead-free organic–inorganic tin halide perovskites for photovoltaic applications *Energy Environ. Sci.* **7** 3061–8

[60] Treglia A, Ambrosio F, Martani S, Folpini G, Barker A J, Albaqami M D, De Angelis F, Poli I and Petrozza A 2022 Effect of electronic doping and traps on carrier dynamics in tin halide perovskites *Mater. Horiz.* **9** 1763–73

[61] Milot R L, Klug M T, Davies C L, Wang Z, Kraus H, Snaith H J, Johnston M B and Herz L M 2018 The effects of doping density and temperature on the optoelectronic properties of formamidinium tin triiodide thin films *Adv. Mater.* **30** 1804506

[62] Dey K, Roose B and Stranks S D 2021 Optoelectronic properties of low-bandgap halide perovskites for solar cell applications *Adv. Mater.* **33** 2102300

[63] Tai Q *et al* 2019 Antioxidant grain passivation for air-stable tin-based perovskite solar cells *Angew. Chem., Int. Ed.* **58** 806–10

[64] Lin Z, Liu C, Liu G, Yang J, Duan X, Tan L and Chen Y 2020 Preparation of efficient inverted tin-based perovskite solar cells via the bidentate coordination effect of 8-hydroxyquinoline *Chem. Commun.* **56** 4007–10

[65] Liu J, Wang S, Zhu W, Tang Z, Ding L and Hao F 2023 Highly symmetric Lewis base coordinated with Sn^{2+} for reducing voltage loss and retarding oxidation in tin-halide perovskite solar cells *Chem. Eng. J.* **453** 139975

[66] Nakamura T, Yakumaru S, Truong M A, Kim K, Liu J, Hu S, Otsuka K, Hashimoto R, Murdey R and Sasamori T 2020 Sn (IV)-free tin perovskite films realized by in situ Sn (0)

nanoparticle treatment of the precursor solution *Nat. Commun.* **11** 3008
[67] Zeng G, Pu D, Huang L, Guan H, Zhou S, Zhou J, Shen W, Li G, Fang G and Ke W 2023 Enhancing the performance of tin-based perovskite solar cells through solvent purification of tin iodide *J. Mater. Chem.* A **11** 11245–53
[68] Gu F, Ye S, Zhao Z, Rao H, Liu Z, Bian Z and Huang C 2018 Improving performance of lead-free formamidinium tin triiodide perovskite solar cells by tin source purification *Sol. RRL* **2** 1800136
[69] Song T-B, Yokoyama T, Stoumpos C C, Logsdon J, Cao D H, Wasielewski M R, Aramaki S and Kanatzidis M G 2017 Importance of reducing vapor atmosphere in the fabrication of tin-based perovskite solar cells *J. Am. Chem. Soc.* **139** 836–42
[70] Wang C, Gu F, Zhao Z, Rao H, Qiu Y, Cai Z, Zhan G, Li X, Sun B and Yu X 2020 Self-repairing tin-based perovskite solar cells with a breakthrough efficiency over 11% *Adv. Mater.* **32** 1907623
[71] Wang C, Zhang Y, Gu F, Zhao Z, Li H, Jiang H, Bian Z and Liu Z 2021 Illumination durability and high-efficiency Sn-based perovskite solar cell under coordinated control of phenylhydrazine and halogen ions *Matter* **4** 709–21
[72] Roy P, Sinha N K, Tiwari S and Khare A 2020 Influence of defect density and layer thickness of absorption layer on the performance of tin based perovskite solar cell *IOP Conf. Ser.: Mater. Sci. Eng.* **798** 012020
[73] Wei M, Xiao K, Walters G, Lin R, Zhao Y, Saidaminov M I, Todorović P, Johnston A, Huang Z and Chen H 2020 Combining efficiency and stability in mixed tin–lead perovskite solar cells by capping grains with an ultrathin 2D layer *Adv. Mater.* **32** 1907058
[74] Meng X, Wu T, Liu X, He X, Noda T, Wang Y, Segawa H and Han L 2020 Highly reproducible and efficient $FASnI_3$ perovskite solar cells fabricated with volatilizable reducing solvent *J. Phys. Chem. Lett.* **11** 2965–71
[75] Su Y, Yang J, Liu G, Sheng W, Zhang J, Zhong Y, Tan L and Chen Y 2022 Acetic acid-assisted synergistic modulation of crystallization kinetics and inhibition of Sn^{2+} oxidation in Tin-based perovskite solar cells *Adv. Funct. Mater.* **32** 2109631
[76] Wang Z, Lin Q, Wenger B, Christoforo M G, Lin Y-H, Klug M T, Johnston M B, Herz L M and Snaith H J 2018 High irradiance performance of metal halide perovskites for concentrator photovoltaics *Nat. Energy* **3** 855–61
[77] Liao M, Yu B B, Jin Z, Chen W, Zhu Y, Zhang X, Yao W, Duan T, Djerdj I and He Z 2019 Efficient and stable $FASnI_3$ perovskite solar cells with effective interface modulation by low-dimensional perovskite layer *ChemSusChem* **12** 5007–14
[78] Wu T, Cui D, Liu X, Meng X, Wang Y, Noda T, Segawa H, Yang X, Zhang Y and Han L 2020 Efficient and stable tin perovskite solar cells enabled by graded heterostructure of light-absorbing layer *Sol. RRL* **4** 2000240
[79] Guo Z, Jena A K, Kim G M and Miyasaka T 2022 The high open-circuit voltage of perovskite solar cells: a review *Energy Environ. Sci.* **15** 3171–222
[80] Caprioglio P, Stolterfoht M, Wolff C M, Unold T, Rech B, Albrecht S and Neher D 2019 On the relation between the open-circuit voltage and quasi-fermi level splitting in efficient perovskite solar cells *Adv. Energy Mater.* **9** 1901631
[81] Liao Y *et al* 2017 Highly oriented low-dimensional Tin halide perovskites with enhanced stability and photovoltaic performance *J. Am. Chem. Soc.* **139** 6693–9
[82] Xu L, Qian M, Zhang C, Lv W, Jin J, Zhang J, Zheng C, Li M, Chen R and Huang W 2020 In situ construction of gradient heterojunction using organic VOx precursor for efficient and stable inverted perovskite solar cells *Nano Energy* **67** 104244
[83] Liu X, Wang Y, Xie F, Yang X and Han L 2018 Improving the performance of inverted formamidinium Tin iodide perovskite solar cells by reducing the energy-level mismatch *ACS Energy Lett.* **3** 1116–21
[84] Cao J, Tai Q, You P, Tang G, Wang T, Wang N and Yan F 2019 Enhanced performance of tin-based perovskite solar cells induced by an ammonium hypophosphite additive *J. Mater. Chem.* A **7** 26580–5
[85] Cao Q *et al* 2024 Co-self-assembled monolayers modified NiOx for stable inverted perovskite solar cells *Adv. Mater.* **36** 2311970
[86] Wang Q, Xu Y Y, Zhang L, Yang A K, Bai T X, Liu F, Lyu M and Zhu J 2022 Guanidinium thiocyanate additive engineering for high-performance $CsPbIBr_2$ solar cells with an efficiency of 10.90% *ACS Appl. Energy Mater.* **5** 3110–8
[87] Lee M, Kim D, Lee Y K, Koo H, Lee K T and Chung I 2020 Indene-C60 bisadduct electron-transporting material with the high LUMO level enhances open-circuit voltage and efficiency of Tin-based perovskite solar cells *ACS Appl. Energy Mater.* **3** 5581–8
[88] Yang P, Sun C, Fu X, Cheng S, Chen J, Zhang H, Nan Z-A, Yang J, Zhao X-J and Xie L-Q 2023 Efficient Tin-based perovskite solar cells enabled by precisely synthesized single-isomer fullerene bisadducts with regulated molecular packing *J. Am. Chem. Soc.* **146** 2494–502